Thermochemical conversion of polyethylene in a fluidized bed: Impact of transition metal-induced oxygen transport on product distribution

Journal of Analytical and Applied Pyrolysis 163 (2022) 105476

Contents lists available at ScienceDirect

Journal of Analytical and Applied Pyrolysis

journal homepage: www.elsevier.com/locate/jaap

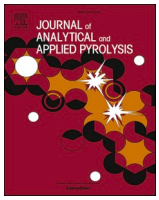

Thermochemical conversion of polyethylene in a fluidized bed: Impact of transition metal-induced oxygen transport on product distribution

Chahat Mandviwala [a,*], Teresa Berdugo Vilches [a], Martin Seemann [a], Robin Faust [b], Henrik Thunman [a]

[a] Department of Space, Earth and Environment (SEE), Division of Energy Technology, Chalmers University of Technology, 412 96 Gothenburg, Sweden
[b] Department of Chemistry and Chemical Engineering, Chalmers University of Technology, 41296 Gothenburg, Sweden

ARTICLE INFO

Keywords:
Dual fluidized bed
Thermochemical conversion
Polyethylene
Transition metals
Oxygen transport
Dehydrogenation

ABSTRACT

Thermochemical conversion in dual fluidized bed (DFB) systems is a potential alternative to the recycling of abundantly available plastic waste. The development of oxygen transport in DFB systems is in most cases unavoidable due to the transition metal content of the bed material as well as the metal fraction in the waste stream. This work investigates the influence of transition metal oxide-induced oxygen transport on the thermochemical conversion of high-density polyethylene, a model plastic feedstock, in a bubbling fluidized bed reactor. Conversion in the reactor at 700 °C was investigated using four different bed materials that had different concentrations of iron oxide. The share of carbon oxides among the gaseous products increased with an increase in the iron oxide content of the bed material. The yield of light olefinic and paraffinic compounds decreased with increased iron oxide content of the bed. The presence of iron oxide in the bed material significantly increased the formation rates of aromatic compounds and solid carbon deposits on the bed material. The observed shift in the product distribution due to oxygen transport follows a dehydrogenation-type reaction mechanism.

1. Introduction

Since the invention of synthetic plastics, approximately 8.3 billion metric tons of plastic materials have been manufactured, as of 2017 [1]. The extremely low cost of producing plastic materials has led to a steady increase in plastic generation over the last few decades, reaching a global production level of 368 million metric tonnes in 2019 [2]. Plastic materials, due to their resistance to biodegradation, constitute a serious waste handling problem. As of Year 2015, approximately 6.3 billion tonnes of plastic waste had been generated, of which around 79% was dumped in landfills or in the natural environment, 12% was incinerated, and only 9% was recycled [1]. If current production and waste management trends continue, approximately 12 billion tonnes of plastic waste will be in the natural environment or landfills by Year 2050 [1].

Currently, the petrochemicals required for the production of plastic materials (e.g., ethylene, propylene, and butenes) are produced mainly from fossil-based aliphatic hydrocarbons [3]. That makes plastic production based on fossil reserves unsustainable. Replacement of fossil-based feedstocks with reusable and recycled resources is, therefore, necessary. In this regard, thermochemical conversion of the abundantly available plastic waste presents an opportunity for the replacement of fossil-based feedstocks [4–9]. High temperature thermochemical processes are aimed at the conversion of plastic materials to light olefins or monomers [5]. Whereas low temperature thermochemical conversion is aimed towards producing liquid hydrocarbons in the range of diesel and gasoline [5]. Implementation of a thermochemical process that aims at producing the feedstocks for new plastic materials will allow the plastic manufacturing industry to become independent of fossil reserves [5].

Waste streams rich in polyolefins such as polyethylene (PE) and polypropylene (PP) represent a promising feedstock for the production of light olefins using high-temperature thermochemical conversion [4,5,9]. These groups of plastic materials account for over 50% of all the plastic materials in the waste stream [1]. In addition, this fraction of the waste stream can be separated from the other fractions (e.g., polyvinyl chloride (PVC), polystyrene (PS), cardboard, paper, metal, etc.) using commercially available density-based separation methods. In reality, the polyolefin-rich plastic waste stream available for thermochemical recycling will be a heterogeneous mixture containing a certain amount of the other fractions present as impurities. In this sense, a fluidized bed

* Corresponding author.
E-mail address: chahat@chalmers.se (C. Mandviwala).

https://doi.org/10.1016/j.jaap.2022.105476
Received 26 November 2021; Received in revised form 9 February 2022; Accepted 12 February 2022
Available online 16 February 2022

is a suitable reactor configuration for the thermochemical conversion of waste plastics due to its heat transfer properties and the ability to treat heterogeneous solid feedstocks [4–9]. Extensive studies have been carried out on the conversion of polyolefins in fluidized bed reactors for producing light olefins [4–9]. For example, Jung and colleagues demonstrated the production of mono aromatics and olefins in a fluidized bed process that used mixed polyolefins as the feedstock [6].

In addition, the selected reactor configuration should be sufficiently robust to remove the solid carbon deposits formed during the thermochemical process. The formation of carbon deposits from liquid and gaseous hydrocarbons in industrial thermochemical processes such as steam cracking and fluid catalytic cracking (FCC) is a common phenomenon [10]. Similarly, thermochemical conversion of polyolefins has also shown a significant formation of solid carbon compared to their fixed carbon content [4,6,8,9]. In addition, the presence of impurities (e.g., paper and cardboard) in the plastic waste will also lead to the formation of solid carbon in a thermochemical process. In fluidized bed reactors, the accumulation of carbon deposits in the bed material leads to the loss of the fluid phase and the heat transfer capacity of the fluidized bed [11]. Continuous removal of the solid carbon formed in the bed material is, therefore, required. The removal of the carbon deposits in the industrial steam cracking and FCC process is done by exposing the carbon deposits to an oxidizing environment [10]. In this sense, besides the intrinsic coverage of heat demand, a dual fluidized bed (DFB) system has another advantage over standalone fluidized bed systems in that a DFB can remove the solid carbon continuously by oxidation within a secondary fluidized bed. In DFB systems, a hot bed material recirculates between the interconnected fluidized beds, i.e., a combustor and a thermochemical reactor (see Fig. 1). This type of configuration, if sealed thoroughly, allows the production of two separate gas streams: flue gas from the combustor; and product gas from the thermochemical reactor. The use of steam or the product gases as the fluidization agent in the thermochemical reactor facilitates the production of nitrogen free product gas. A typical DFB is illustrated in Fig. 1. Fluidized bed conversion of HDPE has been successfully demonstrated in the 2–4-MW_{th} DFB system at Chalmers University of Technology, Gothenburg [5]. Thunman et al. have shown that products derived from the conversion of HDPE in the 2–4-MW_{th} Chalmers DFB system are comparable to the typical product distribution obtained from a tubular naphtha cracker [5]. Wilk and Hofbauer have also investigated the formation of monomers and aromatic hydrocarbon species during the steam gasification of different plastic materials in a 100-kW DFB system [4].

The DFB systems that are dedicated to the thermochemical conversion of waste streams are usually operated with bed materials that are resistant to the impurities present in the feedstock [12]. The bed materials used in such DFB systems are commonly obtained from natural ores, such as silica sand, olivine, bauxite or ilmenite [4,5,13–16]. As these bed materials are natural ores, they contain small amounts of transition metal oxides, such as Fe_2O_3 [13]. When DFB systems are incorporated with bed materials that contain transition metal oxides, transfer of oxygen occurs between the two reactors without any exchange of other gases. This phenomenon is referred to as oxygen transport in the DFB [17]. The flow of transition metal oxides in a DFB system is shown in Fig. 1. The transition metals in a DFB system go through a cycle of oxidation and reduction [16,18]. The transition metals are oxidized in the presence of air in the combustor and reduced in the presence of hydrocarbons and syngas in the thermochemical reactor. Thus, oxygen transport induces an oxidizing environment in the thermochemical reactor, thereby partially or completely oxidizing the feed in the thermochemical reactor. Apart from the inherent properties of the bed material, the ash fraction of the feed used in DFB systems also contributes to the oxygen transfer capability by the formation of an ash layer [14,18].

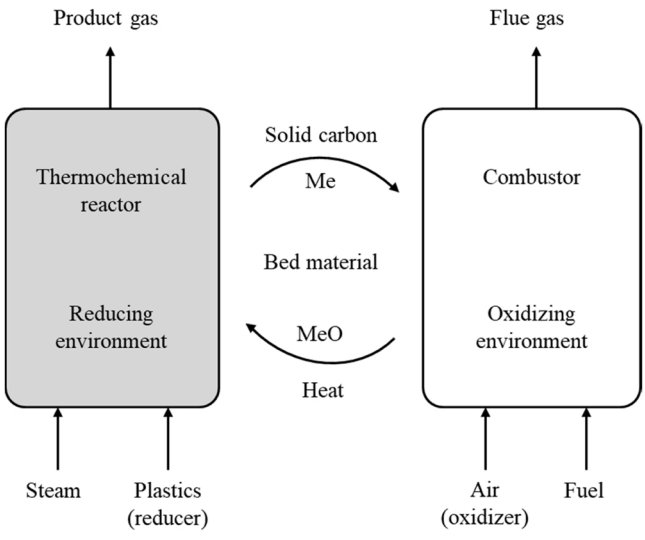

Fig. 1. Schematic of a DFB system illustrating the exchange of bed materials that contain a transition metal oxide (MeO) between the two reactors.

With the increase in oxygen transport from the combustor to the thermochemical reactor, the product distribution from DFB systems has shown increment in CO_x yields compared to the reference cases with minimum oxygen transport [13–16]. Thermochemical conversion of plastic materials is primarily directed towards the production of petrochemical feedstocks, including olefins, paraffins, aromatics and pyrolysis oil. The production of carbon oxides during such a process is, therefore, considered undesirable because it reduces the direct production of the abovementioned economically valuable hydrocarbons. However, the bed material used in a DFB system will exhibit an oxygen transport capability, either due to its inherent transition metal content or due to the presence of transition metals in the feedstock. Partial oxidation of the plastic feed is expected in the presence of transition metal-carrying bed materials, leading to a decrease in the hydrocarbon content of the products. The oxygen transport effect of the bed material is attributed to its ability to undergo redox cycles, in the presence of oxidizing and reducing environments. This effect is maximized in chemical looping processes, such as Chemical Looping Combustion (CLC), Chemical Looping Gasification (CLG), Chemical Looping Reforming (CLR), and Chemical Looping Oxidative Dehydrogenation (CL-OHD), for enhancing the conversion of carbonaceous materials [16–20].

The products obtained from the thermochemical conversion of plastic materials can be categorized into three different groups depending on their hydrogen atom to carbon atom (H/C) ratios:

1. H/C $<$ 2: Aromatics, carbon oxides, solid carbon.
2. H/C $=$ 2: Olefins.
3. H/C $>$ 2: Paraffins.

The distribution of products among these three groups is determined by the reaction conditions and the type of plastic material used [4–8]. For example, thermochemical conversion of LDPE and HDPE favor the production of hydrocarbons with H/C ratio of 2 [4,5]. This is primarily due to the paraffinic structure of PE, which has an H/C ratio of $\sim$ 2. However, the distribution of the products among the abovementioned groups is expected to change due to the partial oxidation of the feedstock caused by the oxygen transport effect of the bed material.

To the best of the authors' knowledge, there are no previous studies reporting on the exclusive impact of oxygen transport linked to the transition metal content of the bed material on the thermochemical conversion of plastic materials in fluidized bed systems. Pissot et al. showed the product distribution derived from CLG of automotive shredder residue (ASR) in the 2–4-MWth Chalmers DFB gasifier and proved the development of oxygen transport properties of the bed material due to the high metal content of the ASR [18]. The increase in oxygen transport was found to increase the extent to which carbon was converted to carbon dioxide in the gasifier. Further, the CL-OHD process

has been used for the dehydrogenation of the light paraffins ethane and propane for the production of ethylene and propylene, respectively, by the means of a transition metal oxide [17,19–21]. CL-OHD of ethane and propane takes place through the following two redox reactions:

$$C_2H_6 + MeO \rightarrow C_2H_4 + Me + H_2O \quad (1)$$

$$C_3H_8 + MeO \rightarrow C_3H_6 + Me + H_2O \quad (2)$$

In the CL-OHD process, the oxygen transport effect of the bed material dehydrogenates the paraffin molecules through oxidation of the hydrogen atoms [17,19–21]. Based on these experiences, oxidation of the carbon atoms in the plastic feed is expected in the presence of a bed material that contains transition metal oxides, as observed in the CLG process. Simultaneously, the increased oxidation of hydrogen atoms can also lead to a dehydrogenation reaction similar to that seen in the CL-OHD. Nonetheless, the thermochemical conversion products are expected to have an average H/C lower than that of the feedstock.

This work aims to study the influence of transition metal-induced oxygen transport on the thermochemical conversion products of PE in a fluidized bed system. A reaction mechanism governing the product distribution in presence of oxygen carrying bed materials is also investigated. Fe_2O_3 was used as model oxygen carrying bed material and virgin HDPE as a model plastic feedstock to minimize the possible influence of other species on the reaction mechanism. The bed materials comprised Al_2O_3 impregnated with Fe_2O_3 at three different concentrations. Al_2O_3 without iron oxide was used as the reference material. In this work, a standalone bubbling fluidized bed (BFB) reactor resembling the thermochemical reactor of a DFB system was used to perform thermochemical conversion of HDPE.

2. Materials and method

2.1. Materials

The HDPE pellets used in this work, with bulk density of 945 kg/m^3 and average pellet size of 2.5 mm were provided by Borealis AB. Aluminum oxide (neutral Al_2O_3, pH 7 in water) with a purity of 99.5% wt. Al_2O_3 and particle size in the range of 40–160 μm was obtained from Sigma-Aldrich. Iron (III) nitrate nonahydrate with a purity of > 98% was obtained from Fisher Scientific. Proximate analysis of the HDPE (as provided by the supplier), along with the carbon and hydrogen contents of the HDPE, is detailed in Table 1. The carbon and hydrogen contents (wt%) were calculated based on the HDPE molecular structure of -[CH_2]- repeating units.

2.2. Bed material preparation and characterization

Al_2O_3 was used as the reference bed material and as the support matrix for impregnating the iron oxide. Bed materials with different contents of iron oxide were prepared by impregnating the Al_2O_3 with an aqueous solution of $Fe(NO_3)_3.9\,H_2O$. Bed materials impregnated with iron nitrate were then dried overnight in an oven at 105 °C, followed by calcination at 700 °C in a BFB reactor. Thus, Fe_2O_3 is formed on the surface of the support according to the following reaction:

Table 1
Properties of the HDPE pellets used in this study.

Proximate analysis	
Moisture content	0.00%
Volatile matter	99.92%
Fixed carbon	0.00%
Ash content	0.08%
Carbon & Hydrogen	
Carbon (C)	85.70%
Hydrogen(H)	14.20%

$$Fe(NO_3)_3 \bullet 9H_2O \xrightarrow{heat} Fe_2O_3 + 3NO_2 + 9H_2O \quad (3)$$

Three bed materials with iron contents of 1%, 2% and 5% by weight were prepared, and hereinafter are referred to as 1Fe/Al_2O_3, 2Fe/Al_2O_3 and 5Fe/Al_2O_3, respectively. The prepared bed materials were investigated using scanning electron microscopy (FEI ESEM Quanta 200), and energy-dispersive x-ray spectroscopy (SEM-EDS) was conducted to investigate the elemental composition. The bed material particles were fixated with epoxy resin and cross-sections were prepared by grinding with silicon carbide sandpaper, prior to the analysis.

2.3. Reactor setup

The experimental setup used in this work is depicted in Fig. 2. The main reactor is a stainless-steel tube with height of 1305 mm and internal diameter (ID) of 88.9 mm. The fluidization gases are introduced separately and mixed homogeneously in the windbox before entering the reactor through the gas distributor plate. The flow of the fluidization gases is controlled by mass flow controllers (MFCs).

The reactor is externally heated with an electric oven. The temperature along the height of the reactor is measured and logged continuously by the thermocouples placed inside of the reactor. Bed material is loaded at the top of the reactor before heating the reactor. The temperature of the bed material, measured by the bottom-most thermocouple (see Fig. 2), is considered the reaction temperature. The temperature in the freeboard was measured by the other two thermocouples. A split stream of the gases leaving the reactor can be sampled through one of the gas sampling ports: h1 to h3 (Fig. 2).

A gas sampling probe is inserted into the reactor through one of the ports, while the remaining ports are closed to prevent the bed material from entering the port. The height of the port is selected depending on the height of the fluidized bed. The probe is heated to 350 °C with an electrical heating band, to avoid condensation of hydrocarbons and steam. The sampled gas is then divided into two split streams, one stream is passed through a gas conditioning system and the other is passed through a solid-phase extraction (SPE) amine column.

The gas conditioning system involves the scrubbing of the sampled gas with isopropanol, followed by drying with glass wool and silica gel. The cold and dry gas is then analyzed in the SICK GMS 820 permanent gas analyzer (SICK AG, Waldkirch, Germany). The SPE amine used is the Supelclean ENVI-Carb/NH2 tube, obtained from Sigma-Aldrich. The gas sampled through the SPE amine is collected in a 0.5-L Tedlar gas bag.

2.4. Chemical looping tests

Appropriate impregnation of the Al_2O_3 with iron oxide was ensured by measuring the oxygen transport capacities of all the impregnated bed materials using chemical looping tests.

The chemical looping tests were carried out in the BFB reactor described in the experimental setup. Bed materials were exposed to a cycle of reduction phase – inert phase – oxidation phase – inert phase for four cycles, to determine their oxygen transport capacities. A mixture of CO and N_2 was used as the fluidizing medium during the reduction phase, only N_2 was used during the inert phase, and air was used during the oxidation phase.

Chemical looping tests were conducted at the bed temperature of 700 °C. The experimental conditions for the chemical looping tests are detailed in Table 2. A slipstream of gases was sampled from the reactor through gas sampling port h2, to measure the CO and CO_2 concentrations using the SICK GMS820 permanent gas analyzer. Fig. 3 shows the concentration profiles of CO and CO_2 during the reduction and the inert stages of the third chemical looping cycle for the 1Fe/Al_2O_3, 2Fe/Al_2O_3 and 5Fe/Al_2O_3 samples. The first and the second cycles gave the same responses as the third cycle. The oxygen transport capacity of each bed material was calculated according to the following equation:

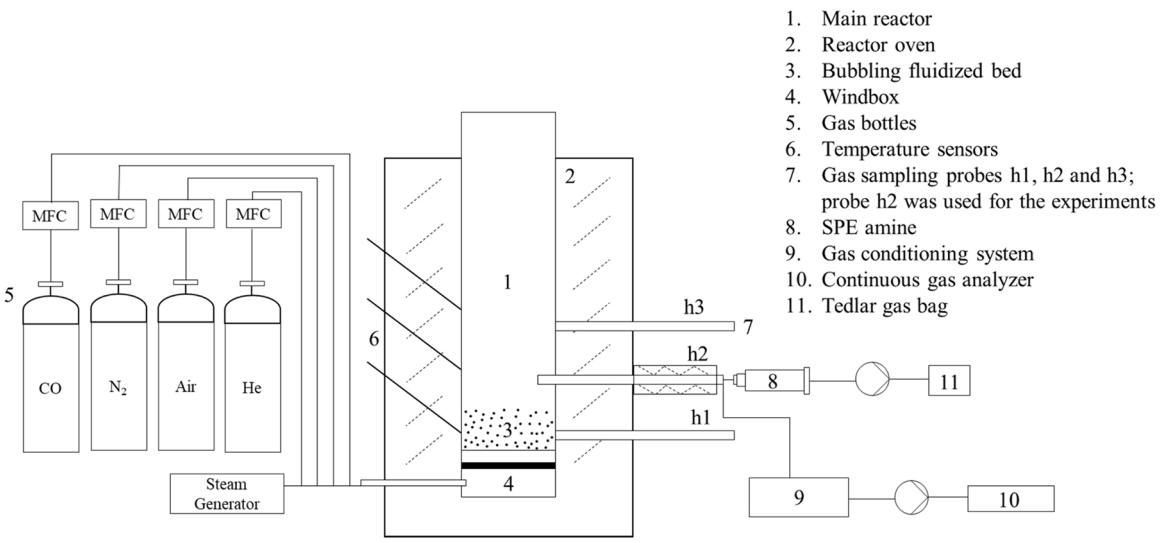

Fig. 2. Schematic of the experimental setup.

Table 2
Experimental conditions for the cyclic chemical looping tests.

Stage	Temperature (°C)	Duration (min)	Gas flow rate
Reduction	700	2	4.0 l_N/min, 25% vol. CO/N_2
Inert	700	1	3.0 l_N/min, 100% N_2
Oxidation	700	3	4.0 l_N/min, Air
Inert	700	1	3.0 l_N/min, 100% N_2

$$\text{oxygen transport capacity, } \%\text{wt} = \frac{M_o}{M_b} \times 100 \quad (4)$$

where M_o is the mass of oxygen released by the bed material as CO_2, and M_b is the total initial mass of the bed material. M_o is calculated from the fraction of CO converted to CO_2 by the bed material during the reduction stage.

2.5. Thermochemical conversion tests

HDPE pellets (2 g per batch) were dropped directly on the top of the hot fluidized bed (700 °C). The experimental conditions were constant for all the four bed materials apart from the minor changes in their initial weight. Five repetitions of each experiment were performed to ensure the repeatability of the experiments. The experimental procedure for each set of experiments is summarized in Table 3.

During the devolatilization and carbon deposits combustion stages of each experiment, helium was used as one of the fluidization gases. The gas flow rate during the devolatilization and the combustion stage corresponds to the fluidization velocity that is 10–12 times the minimum fluidization velocity (u_{mf} = 0.058 m/s) of the bed material. A known volume of helium was introduced as a tracer to determine the total volume of the gases produced during devolatilization and combustion.

Before dropping each batch of HDPE pellets, the bed material was exposed to an oxidizing environment at the same reaction temperature of 700 °C. The temperature of 700 °C was selected to minimize the

Table 3
Experimental procedure for HDPE conversion tests.

Experimental stage	Fluidization gases				Time
	Nitrogen (l_N/min)	Steam (l_N/min)	Air (l_N/min)	Helium (l_N/min)	
Oxidation of the bed material	0.00	0.00	5.00	0.00	Until 20.9% vol. O_2
Devolatilization	2.00	4.00	0.00	0.05	120 s
Carbon deposits combustion	0.00	0.00	5.00	0.05	120 s
Oxidation of the bed material	0.00	0.00	5.00	0.00	Until 20.9% vol. O_2

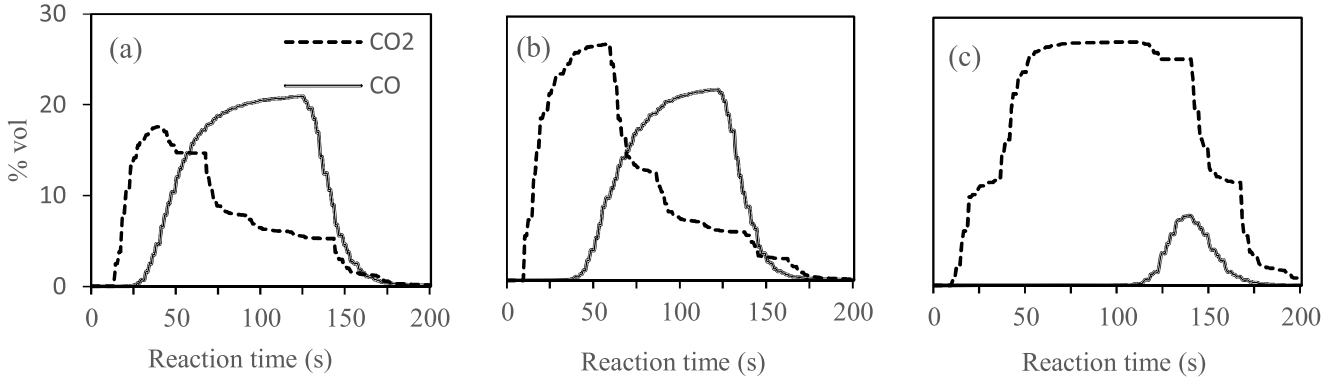

Fig. 3. Measured concentrations of CO and CO_2 (in %vol., dry) during the third cycle of chemical looping tests of each of the impregnated beds: (a) $1Fe/Al_2O_3$; (b) $2Fe/Al_2O_3$; (c) $5Fe/Al_2O_3$.

steam reforming reactions of the produced hydrocarbon species. The temperature in the freeboard was maintained at 695 °C and 690 °C, at heights h2 and h3 (see Fig. 2), respectively. Oxidation of the bed material was achieved by fluidizing the bed material with air, as mentioned in the previous section.

A slipstream of gases leaving the reactor was sampled through sampling port h2 and continuously analyzed for its O_2 concentration (% vol). Complete oxidation was assumed when the O_2 concentration leaving the fluidized bed matched the atmospheric O_2 concentration of 20.9%vol.The bed materials were fully oxidized before each batch of experiments, so as to simulate the conditions of a DFB system, where the bed material enters the thermochemical reactor after being fully oxidized in the combustor.

The thermochemical conversion of HDPE produces products in three different phases:

1. Gas: Volatiles (H_2, CO, C_2H_4, etc.)
2. Liquid: Aromatics (benzene, toluene, styrene, etc.)
3. Solid: Carbon deposits (on the bed material)

The gas and the liquid products leave the reactor along with the fluidization gases, while the solid carbon deposits remain in the reactor together with the bed material.

2.6. Analysis

During the devolatilization of HDPE, one part of the sampled gas was analyzed for its H_2, CO, CO_2 and CH_4 concentrations (%vol.) using the continuous gas analyzer. These gases were monitored continuously to determine the total devolatilization time and to ensure that no volatile gases remained after the sampling time of 120 s.

For a comprehensive analysis of other devolatilized species, the remaining part of the produced gas was sampled through the SPE amine column. Gases leaving the SPE amine were collected in a 0.5-L Tedlar gas bag. The gas bags collected during each experiment were analyzed in the Agilent 490 micro-GC system, to measure the compositions of the gases. The Agilent micro-GC is equipped with four different columns, with a TCD detector for each column. Table 4 gives a summary of the gases measured in the micro-GC system. Since the micro-GC is not able to separate individual C_3, C_4 and C_5 hydrocarbons, these hydrocarbons are collectively represented as C_3H_x, C_4H_x and C_5H_x in the following sections. Detection of aliphatic compounds containing more than five carbon atoms was outside of the scope of the analytic methods used in this work.

The quantification of aromatic hydrocarbons was carried out using the BRUKER GC-FID system in accordance with the solid-phase adsorption (SPA) method described by Israelsson et al. [22]. The measurements performed with the CP-WAX column of the micro-GC system ensured that the benzene and toluene were completely captured and quantified by the SPA method.

Solid carbon deposits remained in the reactor along with the bed material after the devolatilization stage. The yield of carbon deposits was quantified by combusting it in the presence of air and measuring the amounts of CO and CO_2 produced during the process. The fluidization gases were changed from steam and nitrogen to air, in order to combust the carbon deposits in the bed material. Combustion gases were sampled for a period of 120 s and collected in a separate 0.5–L Tedlar gas bag. The composition of the combustion gases collected in the gas bag was measured in the micro-GC system.

Table 4
Gases measured by the Agilent 490 micro-GC system.

Column	Gases	Calibration
CP-Cox	He, H_2, Air (coelution of N_2 and O_2), CO, CH_4	4-point calibration
PoraPLOT U	CO_2, C_2H_4, C_2H_6. C_2H_2, C_3H_x	4-point calibration
CP-WAX 52 CB	Benzene, Toluene	No calibration
CP-Sil 5 CB	C_4H_x, C_5H_x	1-point calibration

2.7. Data evaluation

The results presented in this work were derived from the same sampling, analysis and evaluation methods. As a result, the systematic errors for all the data points are expected to be similar, making the observed trends statistically significant. The datasets presented in the following sections are the mean values derived from multiple repetitions of the experiments. The errors represent the standard deviations among the performed repeats.

The molar yields (mol/kg_{HDPE}) of the gaseous species collected in the Tedlar gas bags were calculated according to the He-tracing method. Eq. (5) was used to calculate the molar yield of all the measured gaseous species.

$$n_i = \frac{c_i}{m_{HDPE}} \times \left(\frac{V_{He-tracing}}{C_{He}}\right) \times \frac{1}{V_m} \quad (5)$$

In Eq. (5), n_i denotes the molar yield and c_i is the concentration of gaseous species *i*. $V_{He\text{-}tracing}$ and C_{He} represent the volume and concentration of the tracer helium gas, respectively. m_{HDPE} is the mass of the HDPE pellets for each batch, and V_m is the molar volume of an ideal gas at 25 °C. The molar yield of each species is then transformed to the corresponding carbon and hydrogen yield based on the total carbon and hydrogen content of the HDPE feed (see Table 1).

3. Results

3.1. Bed material analysis

To confirm the presence of Fe in the Al_2O_3 particles, SEM-EDS was conducted. Fig. 4 shows the back-scattered electron (BSE) signal from a cross-section of the Al_2O_3 particles to which 5%wt. Fe had been added.

The contrast of the BSE images was created by differences in the average atomic weight, i.e., the brightness of the pixels increased with an increase in the atomic weight of the scanned element. Therefore, the epoxy that consists of light elements appears in black and the particles are in brighter shades. As Fe is heavier than Al, the relative Fe content of the particles can be determined from the BSE contrast, whereby the brighter particles contain relatively more Fe. EDS point analysis recorded for the four particles revealed differences in Fe concentration (Table 5). Note that the values in the table are normalized on an O-free and C-free basis, as these elements are challenging to quantify with SEM-EDS. While it is clear that the particles contain different amounts of Fe, all of the particles investigated contain at least 1 at. percentage (at%) Fe. The micrograph acquired at higher magnification [Fig. 4(b)] reveals that the surfaces of the particles exhibit a thin, bright layer that is rich in Fe.

A similar analysis was conducted for the samples with 1 wt% and 2 wt% Fe. As expected, lower concentrations of Fe were found, and some particles only contained Fe in the vicinity of the surface. Although Fe was unevenly distributed and some Al_2O_3 particles appeared to absorb preferentially large quantities of Fe, the presence of Fe was detected on the particle surface for all three samples.

3.2. Oxygen transport capacity

The oxygen transport capacities of all four bed materials used in this work are shown in Fig. 5. The bed material used as the reference was assumed to have oxygen transport capacity of 0%, since it contained < 0.03 wt% Fe_2O_3 (as described by the supplier).

Theoretical values for the oxygen transport capacities were estimated as 0.14, 0.28 and 0.71 wt% (reduction from Fe_2O_3 hematite

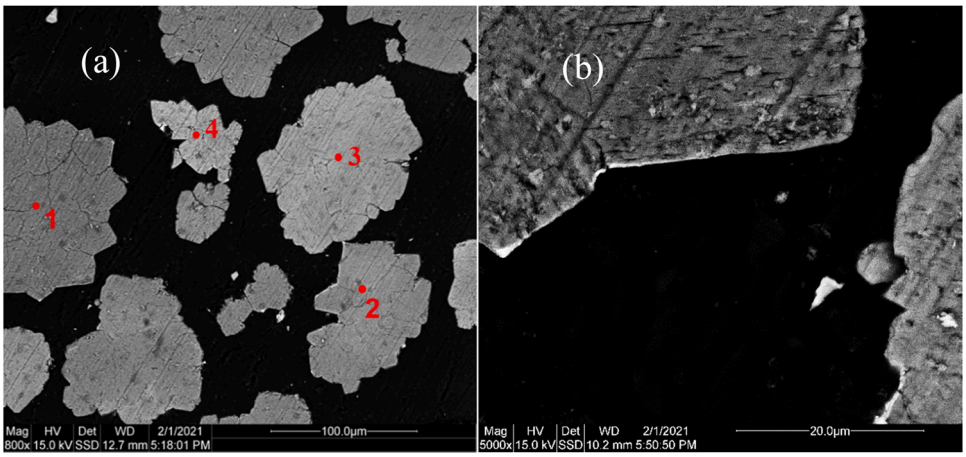

Fig. 4. Back-scattered electron micrographs of the sample in which 5 wt% Fe had been added to the Al_2O_3 particles. EDS point analyses shown in Panel (a) were recorded for the particles and the composition is shown in Table 5. Panels (a) and (b) shows different magnifications of the same SEM image.

Table 5
Concentrations of Al and Fe in atomic percentage (at%) on an O-free and C-free basis recorded at the locations indicated in Fig. 4(a).

Location	Al (at%)	Fe (at%)
1	99	1
2	95	5
3	94	6
4	90	10

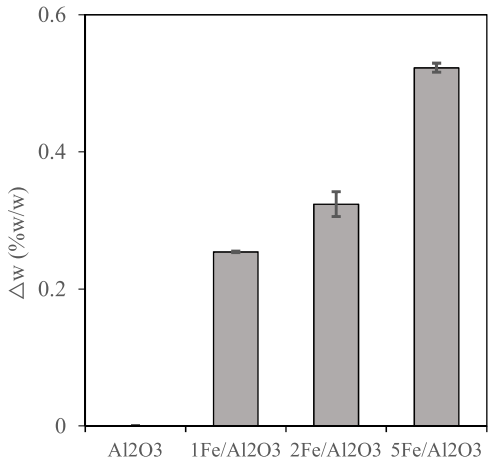

Fig. 5. The oxygen transport capacities of the tested bed materials.

phase to FeO wüstite phase) for $1Fe/Al_2O_3$, $2Fe/Al_2O_3$ and $5Fe/Al_2O_3$, respectively. According to the calculations, the experimental oxygen transport capacities of $1Fe/Al_2O_3$ (0.25%) and $2Fe/Al_2O_3$ (0.32%) were slightly higher than the theoretical values.

This indicates elemental iron formation from the reduced FeO wüstite phase during the chemical looping tests. The increase in oxygen transport capacity with increasing iron content of the bed material ensures proper impregnation of Fe_2O_3 over Al_2O_3.

3.3. Product distribution

The results reported in Table 6 represent the overall carbon balance for all the performed experiments in this work. The error values correspond to the standard deviation among the repetitions of the performed experiments and represent the reproducibility of the experiments. The yields of the hydrocarbon species and carbon oxides are reported as % carbon, by weight (of the carbon content of the feedstock), and the yield of hydrogen gas (H_2) is reported as %hydrogen, by weight (of the hydrogen content of the feedstock). The results obtained with the sampling and analysis employed in this work correspond to the carbon balance closure of 94%, 95%, 88%, and 86% for Al_2O_3, $1Fe/Al_2O_3$, $2Fe/Al_2O_3$, and $5Fe/Al_2O_3$, respectively. The undetected carbon reported in Table 6 is the difference between the total carbon in the feedstock and the amount of carbon measured in the products. The undetected carbon corresponds to the aliphatic hydrocarbon species with more than five carbon atoms that were beyond the scope of the analytical methods used in this work.

The yield of ethylene was similar for Al_2O_3 and $1Fe/Al_2O_3$ at 17.52% and 17.37%, respectively. The other two bed materials, $2Fe/Al_2O_3$ and $5Fe/Al_2O_3$, gave significantly lower ethylene yields of 11.05% and 7.43%, respectively. In all four experiments, aromatic compounds comprised mainly benzene and toluene. The yield of aromatic compounds increased as the iron oxide content of the bed material increased. Thus, the total yield of aromatics increased from 15.03% for Al_2O_3 to 26.98% for $5Fe/Al_2O_3$. The yield of paraffins, including methane and ethane, showed the opposite trend to that of the aromatics. The paraffin yield was highest at 14.84% for Al_2O_3 and lowest at 6.66% for $5Fe/Al_2O_3$. The iron oxide content of the bed material also had a significant impact on the amount of carbon that appeared as carbon oxides among the products of the thermochemical conversion. The combined yields of CO and CO_2 were 4.70% and 13.53% for the bed materials with the lowest and highest iron oxide contents, respectively. The yields of the carbon deposits also increased significantly from 2.19% to 15.50% with the increase (from lowest to highest) in the iron oxide content of the bed material.

The results obtained in this work (Table 6) are reported as the contribution of carbon-containing species (%carbon) to the carbon balance and that of H_2 (%hydrogen) to the hydrogen balance. That gives a clear understanding of the distribution of carbon and hydrogen atoms among the products of thermochemical conversion. Reporting the results as %weight of the feedstock can be misleading, particularly for carbon oxides since the feedstock contains only carbon and hydrogen (see Table 1). Nevertheless, the results reported in Table 6 can be converted to the %weight of the feedstock using the carbon and hydrogen content of the feedstock for a fair comparison with the results reported in the literature.

The yield (as wt% of the feedstock) of ethylene and C_3H_x for Al_2O_3 (17.51 wt% and 11.07 wt%, respectively) and $1Fe/Al_2O_3$ (17.36 wt% and 11.26 wt%, respectively) is comparable to that obtained by Jung. et al. from fluidized bed conversion of polyethylene at 704 °C [6]. The yields reported by Jung. et al. stood at 18.2 wt% and 11.7 wt% for ethylene and propylene, respectively [6]. Zhang. et al. and Elordi. et al.

Table 6
Distribution of the products from the thermochemical conversion of HDPE. Carbon containing species are reported as their contribution (%) to the carbon balance, and H_2 is reported as its contribution (%) to the hydrogen balance.

	Al_2O_3		$1Fe/Al_2O_3$		$2Fe/Al_2O_3$		$5Fe/Al_2O_3$	
%carbon, by weight								
Ethylene	17.52	±0.53	17.37	±1.30	11.05	±0.98	7.43	±1.39
C_3H_x	11.08	±0.28	11.27	±0.83	6.85	±0.52	4.38	±0.82
$C_4H_x + C_5H_x$	30.03	±0.10	19.98	±1.96	15.38	±1.01	11.55	±0.83
Total paraffins	14.84	±0.62	14.07	±0.93	9.91	±0.73	6.66	±0.26
Methane	8.95	±0.36	8.30	±0.55	6.27	±0.49	4.35	±0.66
Ethane	4.78	±0.53	4.65	±0.35	3.02	±0.24	1.91	±0.33
Total aromatics	15.03	±1.48	19.95	±1.78	23.10	±1.26	26.98	±2.17
Benzene	6.06	±0.76	8.26	±0.89	10.19	±0.56	11.41	±0.91
Toluene	3.67	±0.46	5.10	±0.47	6.21	±0.31	6.83	±0.48
Xylene	0.84	±0.09	1.13	±0.11	1.41	±0.14	1.66	±0.12
Styrene	0.84	±0.11	1.11	±0.09	1.46	±0.07	1.58	±0.12
Naphthalene	0.87	±0.11	1.25	±0.08	1.55	±0.12	1.73	±0.15
Others	2.73	±0.34	3.10	±0.34	2.28	±0.19	3.77	±0.31
Total carbon oxides	4.70	±0.01	5.77	±0.37	10.32	±0.89	13.53	±0.59
Carbon monoxide	1.47	±0.03	1.25	±0.08	2.26	±0.21	2.06	±0.18
Carbon dioxide	3.23	±0.04	4.52	±0.24	8.06	±0.69	11.48	±1.00
Carbon deposits	2.19	±0.10	6.59	±0.30	12.08	±0.78	15.50	±0.09
Undetected[a]	5.72	±0.64	6.14	±1.24	11.93	±1.03	14.37	±1.02
%hydrogen, by weight								
Hydrogen (H_2)	10.84	±0.53	8.93	±0.25	14.63	±0.59	14.55	±1.15

[a] Undetected represents the difference between the total carbon in the feedstock and the amount of carbon in the measured products.

obtained a 28 wt% combined yield of ethylene and propylene from fluidized bed conversion of polyethylene at a temperature of 600 °C and 700 °C, respectively [7,23]. The total yield of aromatics reported by Jung. et al. was 13.2 wt% and 17.8 wt% at 704 °C and 728 °C, respectively, which is in line with the yields of aromatics obtained for Al_2O_3 (13.94 wt%) and $1Fe/Al_2O_3$ (18.54 wt%). The yield of aromatics obtained by Elordi. et al. (3.5 wt%) from a conical spouted fluidized bed process was significantly lower than Al_2O_3 and $1Fe/Al_2O_3$ [23]. Although the product distribution obtained with Al_2O_3 and $1Fe/Al_2O_3$, and the previously reported literature showed some similarities, the product distribution obtained with $2Fe/Al_2O_3$ and $5Fe/Al_2O_3$ showed significant deviations [6,7,23]. The product distribution obtained with the oxygen-carrying bed materials $2Fe/Al_2O_3$ and $5Fe/Al_2O_3$ has, in particular, a considerably higher share of aromatics and solid carbon as compared to the previously reported literature [6,7,23]. The shift in the product distribution in the presence of $2Fe/Al_2O_3$ and $5Fe/Al_2O_3$ indicates that the thermochemical conversion of polyethylene in the presence of transition metal oxides follows a different reaction mechanism.

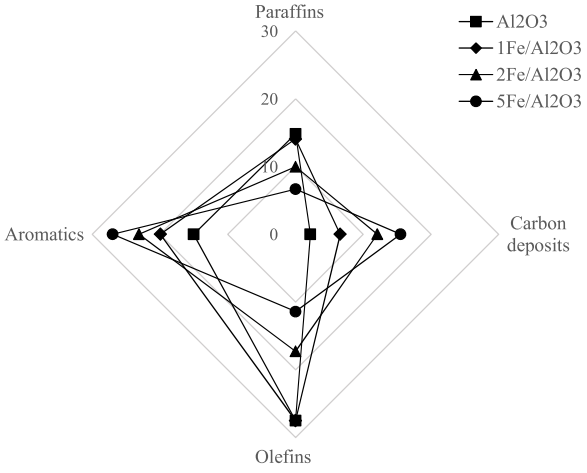

Fig. 6. Yields (%carbon, by weight) of paraffins, olefins, aromatics, and carbon deposits from thermochemical conversion with each of the four bed materials.

4. Discussion

The ability of a bed material to oxidize carbon and hydrogen is usually attributed to its transition metal oxide content. From the results shown in Table 6, it is clear that the oxidation of carbon atoms increases with increases in the iron oxide content of the bed material. However, the extent to which hydrogen atoms are oxidized to H_2O remains unclear. A complete carbon balance and quantification of all olefinic and paraffinic species are required to determine the extent of oxidation of hydrogen atoms.

The yield of hydrocarbon species is expected to decrease with increases in the extent of their oxidation to CO and CO_2. However, the levels of aromatic hydrocarbons showed a significant increase with the increase in oxidation of carbon atoms. A similar trend was observed for the yields of carbon deposits. Fig. 6 shows the trends for aromatics, carbon deposits, olefins and paraffins for thermochemical conversion with each of the four bed materials. It is noteworthy that thermochemical conversion of HDPE in the presence of iron oxide-impregnated bed material favors the formation of species with H/C ratios < 2, whereas the formation of species with H/C ratios ≥ 2 is suppressed.

Fig. 7 shows the H/C ratios of the products obtained through

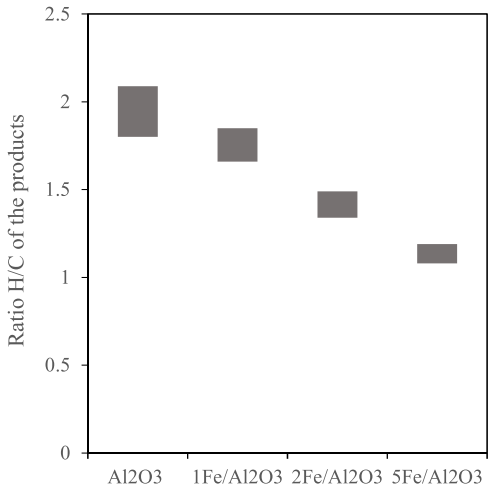

Fig. 7. H/C ratio range of the products obtained from thermochemical conversion with each of the four bed materials.

thermochemical conversion using each of the four bed materials. Since the C_3H_x, C_4H_x and C_5H_x compounds are not known specifically, a range rather than an exact value was calculated for the of H/C ratio. For the purpose of calculating the maximum value of the range, C_3H_x, C_4H_x and C_5H_x were assumed to be C_3H_8, C_4H_{10} and C_5H_{12}, respectively, whereas for calculating the minimum value of the range, they were assumed to be C_3H_4, C_4H_6 and C_5H_8, respectively. It is clear from Fig. 7 that the amount of hydrogen retained by the carbon atoms in the products is affected significantly by the presence of iron oxide in the bed material.

The initial PE polymer chain has a structure composed of -[CH_2]- repeating units with an H/C ratio of 2. In the absence of iron oxide in the bed material, i.e., Al_2O_3, the H/C ratio of the products (1.8–2.1) is very close to that of the initial PE molecule. This ratio decreased in the presence of iron oxide, with the products derived from using the 5Fe/Al_2O_3 bed material showing the lowest H/C ratio range of 1.08 –1.19. This trend is observed mainly because the formation of aromatics, carbon deposits, and carbon oxides with H/C ratio < 2 is favored in the presence of iron oxide.

A similar analysis was conducted for the yield of hydrogen atoms, including all the produced hydrocarbons and hydrogen gas (H_2). A similar H/C ratio to that seen for the products was observed for the yield of hydrogen atoms (Fig. 8). The yield of hydrogen atoms for the reference material (Al_2O_3) was in the range of 95.4–108.8%, indicating no or very low levels of missing hydrogen. The yield of hydrogen atoms for all the iron oxide-bearing bed materials was significantly lower than for the reference case.

The missing hydrogen among the products indicates that hydrogen is oxidized to H_2O along with the oxidation of carbon in the presence of iron oxide. Oxidation of the hydrogen atoms in the feed and the formation of species with H/C ratios < 2 in the presence of oxygen-carrying bed materials can be attributed to a dehydrogenation-type reaction mechanism. Dehydrogenation of the PE molecule in the presence of oxygen-carrying bed materials can be compared to the dehydrogenation of light paraffins (ethane and propane) in the CL-OHD process.

A proposed reaction mechanism based on the results obtained in this work is shown in Figs. 9 and 10. In the presence of a transition metal oxide, the initial polymer chain undergoes dehydrogenation and is depleted of its hydrogen atoms before being broken down into smaller molecules. Oxidation of hydrogen to form H_2O during the process indicates the possibility of OH radical formation during the initial dehydrogenation stage. The unstable OH radical formed during the dehydrogenation step is removed as H_2O after abstracting one more H atom from the PE chain or any other hydrocarbon species. This leads to the formation of carbon-carbon double bonds along the polymer chain.

The formation of aromatic compounds and the solid carbon deposits

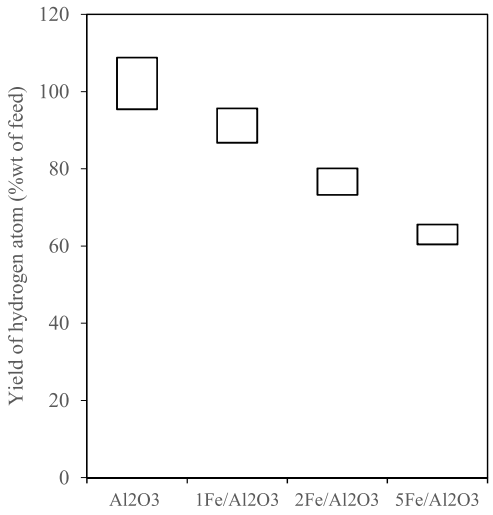

Fig. 8. Range of yields of hydrogen atoms for the four bed materials,.

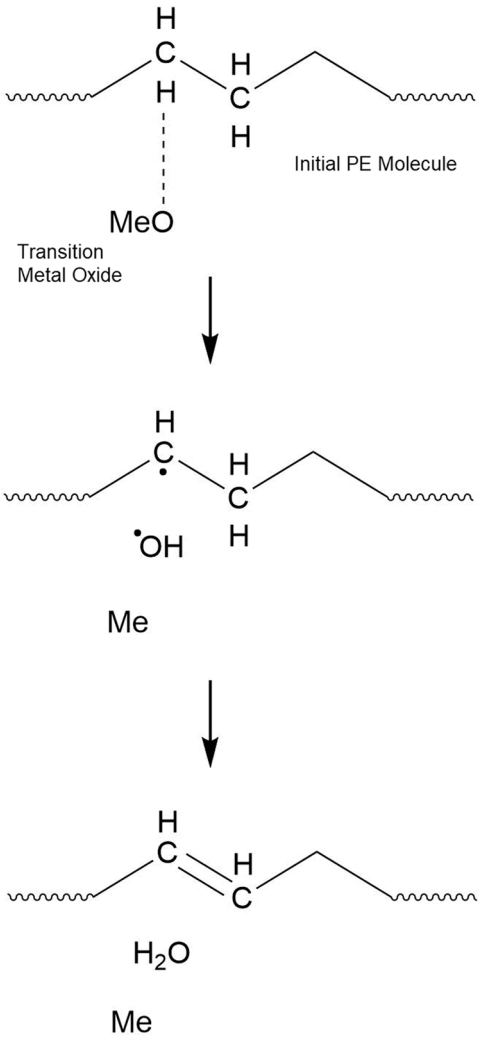

Fig. 9. Dehydrogenation of polyethylene through the formation of OH radicals.

from the dehydrogenated PE molecule can be explained through the reaction mechanism described in Fig. 10. The reaction mechanism proposed here is comparable to the reaction mechanism governing thermal degradation of dehydrochlorinated PVC due to the similarities between the structures of dehydrochlorinated PVC and dehydrogenated PE molecule [24,25]. The formation of aromatic rings proceeds through random scission of the dehydrogenated PE chain followed by cyclization. The formation of the solid carbon deposits proceeds through two different routes: (1) random chain scission of the dehydrogenated PE molecules with subsequent recombination in a mesh-like structure (reaction pathway (3) in Fig. 10); (2) polymerization of the formed aromatic rings (reaction pathway (4b) in Fig. 10). In addition, random scission in the structure of the carbon deposits will also lead to the formation of aromatic rings (reaction pathway (4a) in Fig. 10).

The reaction mechanism proposed here governs the product distribution mainly due to the oxidation of the hydrogen atoms of the feedstock by the bed material. Consequently, the yield of H_2 is expected to decrease with the increase in the oxygen transport capacity of the bed material. The decrease in the yield of H_2 is observed with 1Fe/Al_2O_3 as compared to the reference case. However, a significant increase in the yield of H_2 is observed with the bed materials having higher oxygen transport capacity than 1Fe/Al_2O_3 (see Table 6). This increment in the yield of H_2 is in line with the increase in the yield of the carbon deposits. Reaction pathways (3) and (4a) dominate pathways (2) and (4b) for bed material 2Fe/Al_2O_3 and 5Fe/Al_2O_3, subsequently increasing the yield of H_2.

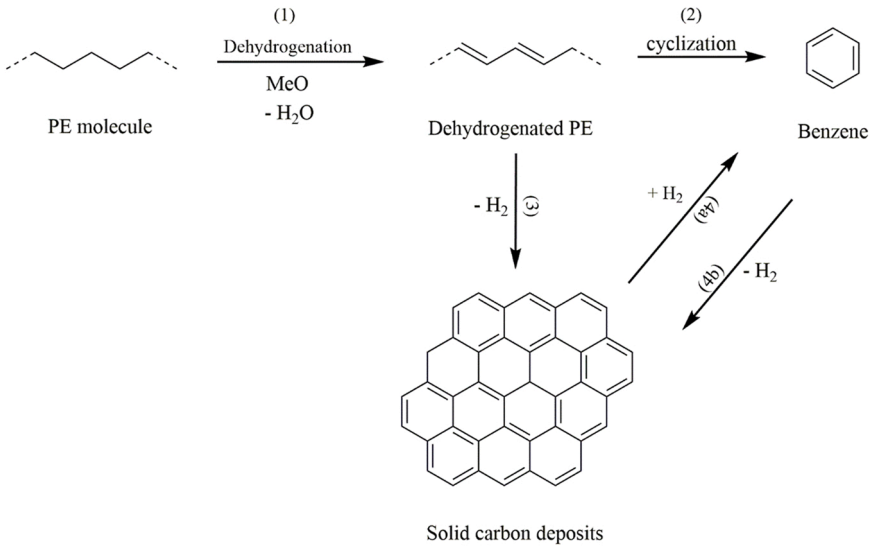

Fig. 10. Reaction mechanism governing the formation of aromatic species and solid carbon from thermochemical conversion of polyethylene, in presence of a transition metal oxide.

The finding that the formation of aromatics and the carbon deposits is affected by the presence of iron oxide on the surface of the bed material is an indication that the proposed dehydrogenation step occurs exclusively on the surface of the bed material.

5. Conclusions

The experimental results obtained in this work reveal that:

- The presence of iron oxide on the surface of the bed material has a significant impact on the product distribution obtained from fluidized bed conversion of HDPE.
- The formation of light olefins and paraffins is suppressed in the presence of bed materials that contain iron oxide.
- The yield of species with H/C ratio < 2, including aromatics, carbon deposits, CO and CO_2, increases with an increase in the iron oxide content of the bed material.
- A dehydrogenation type of mechanism can be used to explain the formation of species with H/C ratio < 2.

The transition metal content of the bed material becomes important for industrial DFB units that aim to produce light olefinic compounds, such as ethylene and propylene, through the thermochemical conversion of plastic materials. Thermochemical conversion of PE in the presence of transition metal oxides is a topic that remains open for further research; the proposed mechanism may be confirmed by the detection of OH radicals in such a system.

CRediT authorship contribution statement

Chahat Mandviwala: Conceptualization, Methodology, Investigation, Data curation, Writing – original draft. **Teresa Berdugo Vilches**: Investigation, Writing – review & editing, Supervision. **Martin Seemann**: Supervision, Writing – review & editing, Project administration. **Robin Faust:** Methodology, Investigation, Writing – original draft. **Henrik Thunman:** Conceptualization, Writing – review & editing, Funding acquisition.

Declaration of Competing Interest

The authors declare that they have no known competing financial interests or personal relationships that could have appeared to influence the work reported in this paper.

Acknowledgments

This work was supported financially by Borealis AB (Project number: 49514–1), the Swedish Gasification Center (SFC), and the Swedish Energy Agency. The authors thank Jessica Bohwalli, Johannes Öhlin and Rustan Hvitt for their technical support during the experiments.

References

[1] R. Geyer, J.R. Jambeck, K.L. Law, Production, use, and fate of all plastics ever made, Sci. Adv. 3 (2017), https://doi.org/10.1126/sciadv.1700782.
[2] Plastics Europe, EU plastics production and demand - first estimates for 2020:: PlasticsEurope, Association of Plastics Manufacturers, 2020.
[3] M. Yang, F. You, Comparative techno-economic and environmental analysis of ethylene and propylene manufacturing from wet shale gas and naphtha, Ind. Eng. Chem. Res. 56 (2017), https://doi.org/10.1021/acs.iecr.7b00354.
[4] V. Wilk, H. Hofbauer, Conversion of mixed plastic wastes in a dual fluidized bed steam gasifier, Fuel 107 (2013), https://doi.org/10.1016/j.fuel.2013.01.068.
[5] H. Thunman, T. Berdugo Vilches, M. Seemann, J. Maric, I.C. Vela, S. Pissot, H.N. T. Nguyen, Circular use of plastics-transformation of existing petrochemical clusters into thermochemical recycling plants with 100% plastics recovery, Sustain. Mater. Technol. 22 (2019), https://doi.org/10.1016/j.susmat.2019.e00124.
[6] S.H. Jung, M.H. Cho, B.S. Kang, J.S. Kim, Pyrolysis of a fraction of waste polypropylene and polyethylene for the recovery of BTX aromatics using a fluidized bed reactor, Fuel Process. Technol. 91 (2010), https://doi.org/10.1016/j.fuproc.2009.10.009.
[7] H. Zhang, J. Nie, R. Xiao, B. Jin, C. Dong, G. Xiao, Catalytic co-pyrolysis of biomass and different plastics (polyethylene, polypropylene, and polystyrene) to improve hydrocarbon yield in a fluidized-bed reactor, Energy Fuels (2014), https://doi.org/10.1021/ef4019299.
[8] S.J. Kern, C. Pfeifer, H. Hofbauer, Cogasification of polyethylene and lignite in a dual fluidized bed gasifier, , Ind. Eng. Chem. Res. 52 (2013), https://doi.org/10.1021/ie303453e.
[9] K. Suresh Kumar Reddy, P. Kannan, A. al Shoaibi, C. Srinivasakannan, Thermal pyrolysis of polyethylene in fluidized beds: Review of the influence of process parameters on product distribution, J. Energy Resour. Technol., Trans. ASME 134 (2012), https://doi.org/10.1115/1.4006790.
[10] Ullmann's Encyclopedia of Industrial Chemistry, 2000. https://doi.org/10.1002/14356007.
[11] B.H. Davis, Fischer-Tropsch synthesis: relationship between iron catalyst composition and process variables, Catal. Today (2003), https://doi.org/10.1016/S0920-5861(03)00304-3.
[12] T. Berdugo Vilches, J. Marinkovic, M. Seemann, H. Thunman, Comparing active bed materials in a dual fluidized bed biomass gasifier: olivine, bauxite, quartz-sand, and ilmenite, Energy Fuels 30 (2016), https://doi.org/10.1021/acs.energyfuels.6b00327.
[13] T. Berdugo Vilches, J. Marinkovic, M. Seemann, H. Thunman, Comparing active bed materials in a dual fluidized bed biomass gasifier: olivine, bauxite, quartz-sand, and ilmenite, Energy Fuels 30 (2016), https://doi.org/10.1021/acs.energyfuels.6b00327.

[14] J. Marinkovic, H. Thunman, P. Knutsson, M. Seemann, Characteristics of olivine as a bed material in an indirect biomass gasifier, Chem. Eng. J. 279 (2015), https://doi.org/10.1016/j.cej.2015.05.061.
[15] T. Berdugo Vilches, M. Seemann, H. Thunman, Influence of in-bed catalysis by ash-coated olivine on tar formation in steam gasification of biomass, Energy Fuels 32 (2018), https://doi.org/10.1021/acs.energyfuels.8b02153.
[16] A. Larsson, M. Israelsson, F. Lind, M. Seemann, H. Thunman, Using ilmenite to reduce the tar yield in a dual fluidized bed gasification system, Energy Fuels 28 (2014), https://doi.org/10.1021/ef500132p.
[17] X. Zhu, Q. Imtiaz, F. Donat, C.R. Müller, F. Li, Chemical looping beyond combustion-a perspective, Energy Environ. Sci. 13 (2020), https://doi.org/10.1039/c9ee03793d.
[18] S. Pissot, T. Berdugo Vilches, J. Maric, I. Cañete Vela, H. Thunman, M. Seemann, Thermochemical recycling of automotive shredder residue by chemical-looping gasification using the generated ash as oxygen carrier, Energy Fuels 33 (2019), https://doi.org/10.1021/acs.energyfuels.9b02607.
[19] L.M. Neal, V.P. Haribal, F. Li, Intensified ethylene production via chemical looping through an exergetically efficient redox scheme, IScience 19 (2019), https://doi.org/10.1016/j.isci.2019.08.039.
[20] S. Yusuf, V. Haribal, D. Jackson, L. Neal, F. Li, Mixed iron-manganese oxides as redox catalysts for chemical looping–oxidative dehydrogenation of ethane with tailorable heat of reactions, Appl. Catal. B: Environ. 257 (2019), https://doi.org/10.1016/j.apcatb.2019.117885.
[21] D. Li, R. Xu, X. Li, Z. Li, X. Zhu, K. Li, Chemical looping conversion of gaseous and liquid fuels for chemical production: a review, Energy Fuels 34 (2020), https://doi.org/10.1021/acs.energyfuels.0c01006.
[22] M. Israelsson, M. Seemann, H. Thunman, Assessment of the solid-phase adsorption method for sampling biomass-derived tar in industrial environments, Energy Fuels 27 (2013), https://doi.org/10.1021/ef401893j.
[23] G. Elordi, M. Olazar, G. Lopez, M. Artetxe, J. Bilbao, Product yields and compositions in the continuous pyrolysis of high-density polyethylene in a conical spouted bed reactor, Ind. Eng. Chem. Res. 50 (2011), https://doi.org/10.1021/ie200186m.
[24] J. Zhou, G. Liu, S. Wang, H. Zhang, F. Xu, TG-FTIR and Py-GC/MS study of the pyrolysis mechanism and composition of volatiles from flash pyrolysis of PVC, J. Energy Inst. 93 (2020), https://doi.org/10.1016/j.joei.2020.07.009.
[25] B. Gui, Y. Qiao, D. Wan, S. Liu, Z. Han, H. Yao, M. Xu, Nascent tar formation during polyvinylchloride (PVC) pyrolysis, Proc. Combust. Inst. 34 (2013), https://doi.org/10.1016/j.proci.2012.08.013.